

## Parity-time symmetry along with nonlocal optical solitons and their active controls in a Rydberg atomic gas

Chao Hang<sup>\*</sup> and Guoxiang Huang<sup>†</sup>

*State Key Laboratory of Precision Spectroscopy, School of Physical and Material Sciences,  
East China Normal University, Shanghai 200062, China  
and NYU-ECNU Institute of Physics at NYU Shanghai, Shanghai 200062, China*



(Received 16 July 2018; published 19 October 2018)

We propose a scheme to realize parity-time ( $\mathcal{PT}$ ) symmetry and nonlocal optical solitons in a cold Rydberg atomic system with electromagnetically induced transparency. We show that a two-dimensional (2D) periodic optical potential with  $\mathcal{PT}$  symmetry can be obtained for the propagation of probe laser field by using an incoherent population pumping between two low-lying levels and spatial modulations of control and assistant laser fields. We also show that, based on the giant nonlocal Kerr nonlinearity originated from the strong, long-range atom-atom interaction, the system supports 2D nonlocal gap solitons with very low light intensity. In particular, we find that the degree of the nonlocality of the Kerr nonlinearity, which can be actively tuned in our system, can be used to manipulate the phase transition of the  $\mathcal{PT}$  symmetry and the behavior of the nonlocal optical solitons. Our study opens a route for developing non-Hermitian nonlinear optics, especially for realizing and controlling high-dimensional weak-light optical solitons through adjustable  $\mathcal{PT}$  symmetry and giant nonlocal optical nonlinearity.

DOI: [10.1103/PhysRevA.98.043840](https://doi.org/10.1103/PhysRevA.98.043840)

### I. INTRODUCTION

In the past two decades, considerable attention has been paid to the investigation on parity-time ( $\mathcal{PT}$ ) symmetry in various physical systems, with the main aim to develop non-Hermitian quantum mechanics [1,2]. It has been shown that non-Hermitian Hamiltonians with  $\mathcal{PT}$  symmetry can exhibit entirely real eigenvalue spectra below certain phase transition points, by which many new and unexpected results have been discovered both theoretically and experimentally (see review articles [3–6] and references therein).

Owing to the fact that the Maxwell equation in electrodynamics under paraxial approximation is mathematically equivalent to the Schrödinger equation in quantum mechanics, optics provides an excellent platform for testing the  $\mathcal{PT}$  symmetric non-Hermitian quantum mechanics. In addition to fundamental interest, the study on optical  $\mathcal{PT}$  symmetry has many important applications, including the realization of nonreciprocal and unidirectional invisible light propagations [7–9], coherent perfect absorbers [10–12], giant light amplification [13], novel lasers [14,15], precision measurement [16,17], and even quantum computation [18]. Novel optical solitons [19], and more generally nonlinear waves, in  $\mathcal{PT}$ -symmetric systems based on  $\mathcal{PT}$  symmetry have also been suggested [4].

It is desirable to have  $\mathcal{PT}$ -symmetric systems that can work at weak-light level. Recently, it has been shown that atomic gases interacting with two or more laser fields are promising candidates for realizing optical  $\mathcal{PT}$  symmetry and

achieving new functionalities for non-Hermitian optics that are not available in conventional  $\mathcal{PT}$  symmetric systems [20–25]. Especially, large, local Kerr nonlinearity and local weak-light solitons in such  $\mathcal{PT}$  symmetric systems have been shown possible [26]. It will be interesting if one can obtain realistic optical systems that not only possess  $\mathcal{PT}$  symmetry, but also support nonlocal Kerr nonlinearity and nonlocal weak-light solitons.

In this work, we propose a scheme to realize  $\mathcal{PT}$  symmetry, nonlocal optical solitons, and their active manipulation in a cold Rydberg atomic gas [27] with electromagnetically induced transparency (EIT). We show that a two-dimensional (2D) periodic optical potential with  $\mathcal{PT}$  symmetry can be created for the propagation of probe laser field through the design of the spatial modulations of control and assistant laser fields, together with an incoherent population pumping between two low-lying levels. Based on the strong, long-range interaction between Rydberg atoms, which can map to a giant nonlocal optical Kerr nonlinearity through the EIT [28–30], we demonstrate that the system supports 2D nonlocal optical gap solitons. We find that the degree of the nonlocality of the nonlocal Kerr nonlinearity, which can be actively tuned in our system, can be used to manipulate the  $\mathcal{PT}$  phase transition and hence the behavior of nonlocal optical solitons.

Before proceeding, we note that nonlinear modes and solitons in  $\mathcal{PT}$ -symmetric systems with nonlocal nonlinearity were considered in Refs. [31–37]. The realization of 1D  $\mathcal{PT}$ -symmetric potential using Rydberg atoms was also suggested recently [38]. However, our work is different from Refs. [31–38]. First, in our work a realistic model for obtaining 2D  $\mathcal{PT}$ -symmetric potential is physically designed, which was absent in Refs. [31–37]. Second, at variance with Ref. [38], in our work a physical mechanism of the probe-field

<sup>\*</sup>chang@phy.ecnu.edu.cn

<sup>†</sup>gxhuang@phy.ecnu.edu.cn

gain necessarily for obtaining the  $\mathcal{PT}$  symmetry is clearly provided. In addition, the nonlocal Kerr nonlinearity is taken into account, nonlocal optical solitons are obtained, and their active control is explored. Third, in our work the possibility for obtaining the giant nonlocal Kerr nonlinearity and nonlocal solitons with very low light intensity is demonstrated, which was not considered in Refs. [31–38]. Fourth, in our work an important parameter, i.e., the degree of nonlocality of the Kerr nonlinearity, is shown to be crucial for actively manipulating the  $\mathcal{PT}$  phase transition and the stability of nonlocal gap solitons. Such result was, however, not provided in Refs. [31–38]. Our study opens an avenue for developing non-Hermitian nonlinear optics, especially for realizing and controlling high-dimensional nonlocal optical solitons, which may have promising applications in optical information processing and transmission.

The article is arranged as follows. In Sec. II, we give a description of the physical model under study. In Sec. III, we discuss the realization of  $\mathcal{PT}$ -symmetric optical potential and its active manipulation. In Sec. IV, nonlocal optical solitons and their active control in the system are studied in detail. Finally, Sec. V summarizes the main results of our work.

## II. MODEL

We start with considering a cold, lifetime-broadened four-level atomic system with an inverted-Y type configuration, shown in Fig. 1(a). The electric field acting with the atomic system reads  $\mathbf{E} = \mathbf{E}_p + \mathbf{E}_c + \mathbf{E}_a$ , with  $\mathbf{E}_\alpha = \mathbf{e}_\alpha \mathcal{E}_\alpha \exp[i(\mathbf{k}_\alpha \cdot \mathbf{r} - \omega_\alpha t)] + \text{H.c.}$  ( $\mathbf{e}_\alpha$  are unit polarization vectors;  $\mathcal{E}_\alpha$  are field amplitudes). Here, a weak, spatially focused probe laser field  $\mathbf{E}_p$  (with wave number  $k_p = \omega_p/c$ , angular frequency  $\omega_p$ , and half Rabi frequency  $\Omega_p$ ) couples the ground state  $|1\rangle$  to the intermediate state  $|3\rangle$ ; a strong control laser field  $\mathbf{E}_c$  (with wave number  $k_c = \omega_c/c$ , angular frequency  $\omega_c$ , and half Rabi frequency  $\Omega_c$ ) couples the low-lying state  $|2\rangle$  and the state  $|3\rangle$ .  $\Delta_3$ ,  $\Delta_2$ , and  $\Delta_4$  are respectively one- and two-photon detunings;  $\Gamma_{13}$ ,  $\Gamma_{23}$ , and  $\Gamma_{34}$  are respectively the spontaneous-emission decay rates from  $|3\rangle$  to  $|1\rangle$ ,  $|3\rangle$  to  $|2\rangle$ , and  $|4\rangle$  to  $|3\rangle$ . States  $|1\rangle$ ,  $|2\rangle$ ,  $|3\rangle$  and the probe and control fields constitute a standard  $\Lambda$ -type EIT configuration. The  $\Lambda$ -type EIT is, however, dressed by a high-lying Rydberg state  $|4\rangle$  (with large principal quantum number  $n$ ), which is far off-resonantly (i.e.,  $\Delta_3 + \Delta_4 \gg \Omega_a$ ) coupled to  $|3\rangle$  through an assisted laser field  $\mathbf{E}_a$  (with wave number  $k_a = \omega_a/c$ , angular frequency  $\omega_a$ , and half Rabi frequency  $\Omega_a$ ). The reason for using the Rydberg-dressed EIT is to exploit the advantages of EIT (which can suppress largely the absorption of the probe field due to spontaneous emission) and the Rydberg state (which can provide a giant nonlocal Kerr nonlinearity mapped by atom-atom interaction).

One of our aims is to realize an optical  $\mathcal{PT}$  symmetry in this (weakly absorbed) Rydberg-dressed EIT system, for which a gain to the probe field must be provided. To this end, we assume there is an incoherent population pumping (with pumping rate  $\Gamma_{21}$ ) coupled to the two low-lying states  $|1\rangle$  and  $|2\rangle$ . Note that the incoherent population pumping may be realized by using many techniques, such as intense atomic resonance spectrum lines emitted from hollow-cathode lamps or from microwave discharge lamps [39]. In addition,

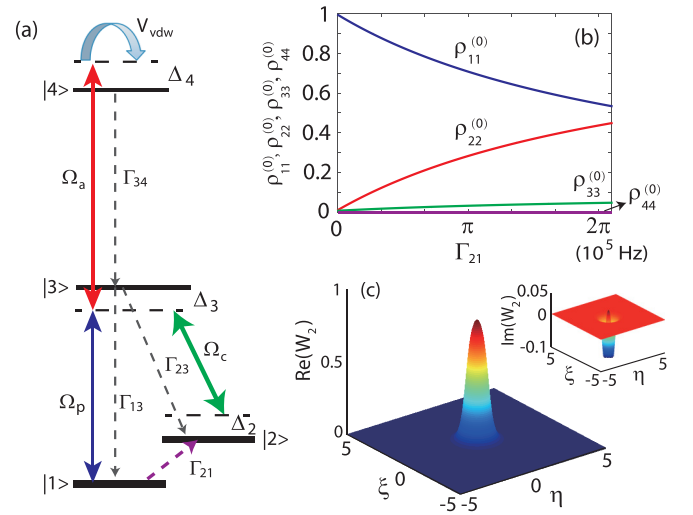


FIG. 1. (a) Level diagram and excitation scheme of the Rydberg-dressed EIT. States  $|1\rangle$ ,  $|2\rangle$ ,  $|3\rangle$  constitute a standard  $\Lambda$ -type EIT configuration, where the probe field (half Rabi frequency  $\Omega_p$ ) couples the transition  $|1\rangle \leftrightarrow |3\rangle$ , and the control field (half Rabi frequency  $\Omega_c$ ) couples the transition  $|2\rangle \leftrightarrow |3\rangle$ .  $\Delta_j$  are detunings and  $\Gamma_{ij}$  are the spontaneous-emission decay rate from  $|i\rangle$  to  $|j\rangle$ . The  $\Lambda$ -type EIT is dressed by a high-lying Rydberg state  $|4\rangle$ , which is far off-resonantly ( $\Delta_3 + \Delta_4 \gg \Omega_a$ ) coupled to the state  $|3\rangle$  through an assisted laser field (half Rabi frequency  $\Omega_a$ ). An incoherent pumping (with pumping rate  $\Gamma_{21}$ ) is used to pump atoms from  $|1\rangle$  to  $|2\rangle$ , providing a gain for the probe field. The control and the assisted fields are assumed to be spatially modulated. The interaction between Rydberg atoms is described by the van der Waals potential  $V_{\text{vdw}} \equiv \hbar V(\mathbf{r}' - \mathbf{r})$ , with  $V(\mathbf{r}' - \mathbf{r}) = C_6/|\mathbf{r}' - \mathbf{r}|^6$ . (b) Populations  $\rho_{jj}^{(0)}$  ( $j = 1, 2, 3, 4$ ) of atoms at different levels as functions of the incoherent population pumping rate  $\Gamma_{21}$ . For  $\Gamma_{21} = 0$ , all populations are in the ground state  $|1\rangle$ ; however, when  $\Gamma_{21} \neq 0$ , we have  $\rho_{33}^{(0)} \neq 0$ . (c) Spatial distributions of the real and imaginary parts of the nonlocal nonlinear coefficient  $W_2$ , i.e.,  $\text{Re}(W_2)$  and  $\text{Im}(W_2)$ , in the plane of dimensionless spatial coordinates  $\xi = x/R_\perp$  and  $\eta = y/R_\perp$ .

the control and the assisted fields are assumed to be spatially periodic modulated (see below).

The dynamics of the system is described by the Hamiltonian  $\hat{H} = \mathcal{N}_a \int d^3\mathbf{r} \hat{\mathcal{H}}(\mathbf{r}, t)$ , with  $\hat{\mathcal{H}}(\mathbf{r}, t)$  the Hamiltonian density and  $\mathcal{N}_a$  the atom density. Under electric-dipole and rotating-wave approximations, the Hamiltonian density in the interaction picture reads

$$\begin{aligned} \hat{\mathcal{H}}(\mathbf{r}, t) = & \sum_{j=1}^4 \hbar \Delta_j \hat{S}_{jj}(\mathbf{r}, t) - \hbar [\Omega_p \hat{S}_{13}(\mathbf{r}, t) + \Omega_a \hat{S}_{34}(\mathbf{r}, t) \\ & + \Omega_c \hat{S}_{23}(\mathbf{r}, t) + \text{H.c.}] \\ & + \mathcal{N}_a \int d^3\mathbf{r}' \hat{S}_{44}(\mathbf{r}', t) \hbar V(\mathbf{r}' - \mathbf{r}) \hat{S}_{44}(\mathbf{r}, t), \quad (1) \end{aligned}$$

where  $\hat{S}_{jl} = |l\rangle\langle j| \exp[i(\mathbf{k}_l - \mathbf{k}_j) \cdot \mathbf{r} - (\omega_l - \omega_j + \Delta_l - \Delta_j)t]$  is the transition operator related to the states  $|j\rangle$  and  $|l\rangle$ , satisfying the commutation relation  $[\hat{S}_{jl}(\mathbf{r}, t), \hat{S}_{\mu\nu}(\mathbf{r}', t)] = (1/\mathcal{N}_a) \delta(\mathbf{r} - \mathbf{r}') [\delta_{j\nu} \hat{S}_{\mu l}(\mathbf{r}', t) - \delta_{\mu l} \hat{S}_{j\nu}(\mathbf{r}', t)]$ , with  $\hbar \omega_j$  the eigenergy of the level  $|j\rangle$ ,  $\Delta_3 = (\omega_3 - \omega_1) - \omega_p$  the one-photon detuning,  $\Delta_2 = \omega_p - \omega_c - (\omega_2 - \omega_1)$  the two-photon

detuning, and  $\Delta_4 = \omega_p + \omega_a - (\omega_4 - \omega_1)$  the two-photon detuning;  $\Omega_p = (\mathbf{e}_p \cdot \mathbf{p}_{31})\mathcal{E}_p/\hbar$ ,  $\Omega_c = (\mathbf{e}_c \cdot \mathbf{p}_{32})\mathcal{E}_c/\hbar$ , and  $\Omega_a = (\mathbf{e}_a \cdot \mathbf{p}_{43})\mathcal{E}_a/\hbar$  are respectively half Rabi frequencies of the probe, control, and assisted fields, with  $\mathbf{p}_{ij}$  the electric dipole matrix elements associated with the transition  $|i\rangle \leftrightarrow |j\rangle$ . The last term in the Hamiltonian (1) is the contribution due to atom-atom interaction. The interaction between the Rydberg

atom at position  $\mathbf{r}$  and the one at position  $\mathbf{r}'$  is described by the long-range potential  $\hbar V(\mathbf{r}' - \mathbf{r})$ , with  $V(\mathbf{r}' - \mathbf{r}) = C_6/|\mathbf{r}' - \mathbf{r}|^6$  ( $C_6$  is called dispersion parameter and could be positive or negative).

From the Hamiltonian given above, we obtain the optical Bloch equations of the density-matrix elements,  $\rho_{jl} \equiv \langle \hat{S}_{jl} \rangle$ , with the form

$$i \frac{\partial}{\partial t} \rho_{11} + i\Gamma_{21}\rho_{11} - i\Gamma_{13}\rho_{33} - \Omega_p\rho_{13} + \Omega_p^*\rho_{31} = 0, \quad (2a)$$

$$i \frac{\partial}{\partial t} \rho_{22} - i\Gamma_{21}\rho_{11} - i\Gamma_{23}\rho_{33} - \Omega_c\rho_{23} + \Omega_c^*\rho_{32} = 0, \quad (2b)$$

$$i \frac{\partial}{\partial t} \rho_{33} + i\Gamma_{33}\rho_{33} - i\Gamma_{34}\rho_{44} + \Omega_p\rho_{13} - \Omega_p^*\rho_{31} + \Omega_c\rho_{23} - \Omega_c^*\rho_{32} - \Omega_a\rho_{34} + \Omega_a^*\rho_{43} = 0, \quad (2c)$$

$$i \frac{\partial}{\partial t} \rho_{44} + i\Gamma_{34}\rho_{44} + \Omega_a\rho_{34} - \Omega_a^*\rho_{43} = 0, \quad (2d)$$

$$\left( i \frac{\partial}{\partial t} + d_{21} \right) \rho_{21} + \Omega_c^*\rho_{31} - \Omega_p\rho_{23} = 0, \quad (2e)$$

$$\left( i \frac{\partial}{\partial t} + d_{31} \right) \rho_{31} + \Omega_p(\rho_{11} - \rho_{33}) + \Omega_c\rho_{21} + \Omega_a^*\rho_{41} = 0, \quad (2f)$$

$$\left( i \frac{\partial}{\partial t} + d_{41} \right) \rho_{41} + \Omega_a\rho_{31} - \Omega_p\rho_{43} - \mathcal{N}_\alpha \int d^3\mathbf{r}' V(\mathbf{r}' - \mathbf{r}) \rho_{44,41}(\mathbf{r}', \mathbf{r}, t) = 0, \quad (2g)$$

$$\left( i \frac{\partial}{\partial t} + d_{32} \right) \rho_{32} + \Omega_p\rho_{12} + \Omega_c(\rho_{22} - \rho_{33}) + \Omega_a^*\rho_{42} = 0, \quad (2h)$$

$$\left( i \frac{\partial}{\partial t} + d_{42} \right) \rho_{42} + \Omega_a\rho_{32} - \Omega_c\rho_{43} - \mathcal{N}_\alpha \int d^3\mathbf{r}' V(\mathbf{r}' - \mathbf{r}) \rho_{44,42}(\mathbf{r}', \mathbf{r}, t) = 0, \quad (2i)$$

$$\left( i \frac{\partial}{\partial t} + d_{43} \right) \rho_{43} + \Omega_a(\rho_{33} - \rho_{44}) - \Omega_p^*\rho_{41} - \Omega_c^*\rho_{42} - \mathcal{N}_\alpha \int d^3\mathbf{r}' V(\mathbf{r}' - \mathbf{r}) \rho_{44,43}(\mathbf{r}', \mathbf{r}, t) = 0, \quad (2j)$$

where  $d_{jl} = \Delta_j - \Delta_l + i\gamma_{jl}$ , with  $\gamma_{ij} = (\Gamma_i + \Gamma_j)/2 + \gamma_{ij}^{\text{col}}$ . Here  $\Gamma_j = \sum_{i < j} \Gamma_{ij}$ , with  $\Gamma_{ij}$  the spontaneous emission decay rate, and  $\gamma_{ij}^{\text{col}}$  the dephasing rate from  $|j\rangle$  to  $|i\rangle$ . In Eqs. (2g), (2i), and (2j), we have used the notation  $\rho_{j\ell,\mu\nu}(\mathbf{r}', \mathbf{r}, t) \equiv \langle \hat{S}_{j\ell}(\mathbf{r}', t) \hat{S}_{\mu\nu}(\mathbf{r}, t) \rangle$  [40].

The wave equation of the probe field is described by the Maxwell equation, which under slowly varying amplitude approximation reads

$$i \left( \frac{\partial}{\partial z} + \frac{1}{c} \frac{\partial}{\partial t} \right) \Omega_p + \frac{1}{2k_p} \left( \frac{\partial^2}{\partial x^2} + \frac{\partial^2}{\partial y^2} \right) \Omega_p + \frac{k_p}{2} \chi_p \Omega_p = 0, \quad (3)$$

where  $\chi_p = \mathcal{N}_\alpha (\mathbf{e}_p \cdot \mathbf{p}_{13})^2 \rho_{31} / (\epsilon_0 \hbar \Omega_p)$  is the probe-field susceptibility. The second term on the left-hand side of Eq. (3) describes the diffraction effect of the probe field. Note that for convenience and without loss of generality, the propagation direction of the probe field is assumed to along  $z$  direction, i.e.,  $\mathbf{k}_p = (0, 0, k_p)$ . To suppress the Doppler effect, we choose  $\mathbf{k}_c = (0, 0, k_c)$  and  $\mathbf{k}_a = (0, 0, -k_a)$ ; in addition, since we are interested in a stationary state of the system, the time derivatives in the Maxwell-Bloch (MB) Eqs. (2) and (3) can be neglected (i.e.,  $\partial/\partial t = 0$ ), which is valid if the probe, control, and assisted fields have long enough time durations.

For a realistic system, say, the  $^{88}\text{Sr}$  system as we proposed below, the probe, control, and assisted fields can be treated as time-independent ones if their durations are much longer than  $1/\Gamma_{34} \approx 10 \mu\text{s}$ .

Since the probe field is weak, the population in atomic levels changes not much when the probe field is applied to the system, and hence a perturbation expansion can be employed to solve the Bloch Eq. (2) [41]. Hence by assuming  $\Omega_p = \epsilon \Omega_p^{(1)} + \epsilon^2 \Omega_p^{(2)} + \dots$  and  $\rho_{jl} = \rho_{jl}^{(0)} + \epsilon \rho_{jl}^{(1)} + \dots$  ( $\epsilon$  is the small parameter characterizing the typical amplitude of the probe field), substituting them into Eq. (2), and comparing coefficients of  $\epsilon^m$  ( $m = 0, 1, \dots$ ), we obtain a set of equations for  $\rho_{jl}^{(m)}$ , which can be solved order by order.

The zeroth-order ( $m = 0$ ) equations and their solution, which describe the case when the probe field is not applied (i.e.,  $\Omega_p = 0$ ), are presented in Appendix A. The key parameter in the solution is the incoherent population pumping rate (i.e.,  $\Gamma_{21}$ ). If  $\Gamma_{21} = 0$ , one has  $\rho_{11}^{(0)} = 1$  and all other  $\rho_{jl}^{(0)} = 0$ . In this case, the system has no gain to the probe field. However, when  $\Gamma_{21} \neq 0$ , we have  $\rho_{33}^{(0)} \neq 0$ , and hence a gain to the probe field will be realized when the probe field is coupled to the states  $|1\rangle$  and  $|3\rangle$  (which is necessary to get a  $\mathcal{PT}$  symmetry in the system). Furthermore, for  $(\Delta_3 + \Delta_4)/\Omega_a \gg 1$ , the population in the Rydberg state  $|4\rangle$  is approximately zero

(i.e.,  $\rho_{44}^{(0)} = 0$ ), which means Rydberg-dressed EIT can be obtained.

Shown in Fig. 1(b) is populations  $\rho_{jj}^{(0)}$  ( $j = 1, 2, 3, 4$ ) as functions of  $\Gamma_{21}$ . For a better illustration, we have taken a laser-cooled strontium ( $^{88}\text{Sr}$ ) atomic gas as a realistic candidate for our theoretical model described above. The assigned atomic levels are  $|1\rangle = |5S_{1/2}, F = 1\rangle$ ,  $|2\rangle = |5S_{1/2}, F = 2\rangle$ ,  $|3\rangle = |5P_{3/2}, F = 3\rangle$ , and  $|4\rangle = |nS_{1/2}\rangle$ . For main quantum number  $n = 60$ , the dispersion parameter is  $C_6 \approx -2\pi \times 81.6 \text{ GHz } \mu\text{m}^6$ . The incoherent population pumping rate is  $\Gamma_{21} \approx 2\pi \times 0.1 \text{ MHz}$ ; spontaneous emission decay rates are respectively  $\Gamma_3 = \Gamma_{31} + \Gamma_{32} \approx 2\pi \times 16 \text{ MHz}$  and  $\Gamma_4 = \Gamma_{34} \approx 2\pi \times 16.7 \text{ kHz}$ . Detunings are  $\Delta_2 = 1.674 \times 10^6 \text{ s}^{-1}$ ,  $\Delta_3 = 9.665 \times 10^7 \text{ s}^{-1}$ , and  $\Delta_4 = 1.335 \times 10^7$ . Other parameters read  $\mathcal{N}_a = 1.0 \times 10^{12} \text{ cm}^{-3}$ ,  $\Omega_c = \Omega_{c0} = 1.5 \times 10^7 \text{ s}^{-1}$ , and  $\Omega_a = \Omega_{a0} = 1.0 \times 10^7 \text{ s}^{-1}$ . Note that with the above parameters we have  $(\Delta_3 + \Delta_4)/\Omega_a = 11 \gg 1$ , so the system works in the regime of Rydberg-dressed EIT.

The first ( $m = 1$ ) order solution describes the linear excitation of the system, which reads  $\rho_{21}^{(1)} = \alpha_{21}^{(1)}\Omega_p$ ,  $\rho_{31}^{(1)} = \alpha_{31}^{(1)}\Omega_p$ , and  $\rho_{41}^{(1)} = \alpha_{41}^{(1)}\Omega_p$ , with other density-matrix elements being zero. With the solutions at the zero and first orders given above, one can go to the second and third orders, with explicit expressions of equations and solutions given in Appendix A. The solution of  $\rho_{31}^{(3)}$  is found to have the form  $\rho_{31}^{(3)} = \alpha_{31,1}^{(3)}|\Omega_p|^2\Omega_p + \mathcal{N}_a \int d^3\mathbf{r}' V(\mathbf{r}' - \mathbf{r})\alpha_{31,2}^{(3)}(\mathbf{r}')|\Omega_p(\mathbf{r}')|^2\Omega_p(\mathbf{r})$ , with  $\alpha_{31,1}^{(3)} = [d_{21}d_{41}(\alpha_{33}^{(2)} - \alpha_{11}^{(2)}) - d_{41}\Omega_c\alpha_{23}^{(2)} - d_{21}\Omega_a^*\alpha_{43}^{(2)}]/D_2$  and  $\alpha_{21,2}^{(3)} = d_{21}\Omega_a^*\alpha_{14}^{(2)}\alpha_{41,41}^{(2)}/D_2$  [42]. With the solution of  $\rho_{31}$  exact to the third order, the susceptibility of the probe field can be expressed as

$$\chi_p = \chi_p^{(1)} + \chi_{p,1}^{(3)}|\Omega_p|^2 + \int d^3\mathbf{r}' \chi_{p,2}^{(3)}(\mathbf{r}' - \mathbf{r})|\Omega_p(\mathbf{r}')|^2, \quad (4)$$

with  $\chi_p^{(1)} = \mathcal{N}_a|\mathbf{e}_p \cdot \mathbf{p}_{12}|^2\alpha_{31}^{(1)}/(\epsilon_0\hbar)$ ,  $\chi_{p,1}^{(3)} = \mathcal{N}_a|\mathbf{e}_p \cdot \mathbf{p}_{12}|^2\alpha_{31,1}^{(3)}/(\epsilon_0\hbar)$ , and  $\chi_{p,2}^{(3)}(\mathbf{r}' - \mathbf{r}) = \mathcal{N}_a^2|\mathbf{e}_p \cdot \mathbf{p}_{12}|^2\alpha_{31,2}^{(3)}V(\mathbf{r}' - \mathbf{r})/(\epsilon_0\hbar)$ . We assume that the spatial length of the probe pulse in  $z$  direction is much larger than the range of atom-atom interactions, so that a local approximation along the  $z$  direction can be made [43]. Hence the last term on the right-hand side of Eq. (4) can be reduced as  $\int d^3\mathbf{r}' \chi_{p,2}^{(3)}(\mathbf{r}' - \mathbf{r})|\Omega_p(\mathbf{r}')|^2 = \int \int dx' dy' \tilde{\chi}_{p,2}^{(3)}(x' - x, y' - y)|\Omega_p(x', y', z)|^2$ , with  $\tilde{\chi}_{p,2}^{(3)}(x' - x, y' - y) = \int dz' \chi_{p,2}^{(3)}(\mathbf{r}' - \mathbf{r})$ .

Substituting Eq. (4) into Eq. (3) we obtain

$$i \frac{\partial \Omega_p}{\partial z} + \frac{1}{2k_p} \left( \frac{\partial^2 \Omega_p}{\partial x^2} + \frac{\partial^2 \Omega_p}{\partial y^2} \right) + \frac{k_p}{2} \chi_p^{(1)} \Omega_p + \frac{k_p}{2} \left( \chi_{p,1}^{(3)} |\Omega_p|^2 + \int \int dx' dy' \tilde{\chi}_{p,2}^{(3)}(x' - x, y' - y) |\Omega_p(x', y', z)|^2 \right) \Omega_p = 0, \quad (5)$$

where  $\chi_p^{(1)}$  is linear susceptibility and  $\chi_{p,1}^{(3)}$  is the local nonlinear susceptibility, appearing in conventional EIT systems [26];  $\tilde{\chi}_{p,2}^{(3)}$  describes a nonlocal nonlinear susceptibility, contributed by the atom-atom interaction in the Rydberg gas. An important point here is that the local Kerr nonlinearity

is proportional to the atomic density, i.e.,  $\chi_{p,1}^{(3)} \propto \mathcal{N}_a$ , and it becomes vanishing when  $\Delta_2 = 0$ . However, the nonlocal Kerr nonlinearity is proportional to  $\chi_{p,2}^{(3)} \propto \mathcal{N}_a^2$ , and it does not vanish when  $\Delta_2 = 0$  [41]. Thus the nonlocal Kerr nonlinearity can be much larger than the local one for large atom density. Furthermore,  $\chi_{p,2}^{(3)} \propto C_6$ , which increases rapidly when the main quantum number  $n$  increases [27]. With the parameters of  $^{88}\text{Sr}$  given above, the maximum of  $\chi_{p,2}^{(3)}$  can reach the value of approximately  $(2.6 + i0.5) \times 10^{-12} \text{ Hz}^{-2}$ . Thus we have a giant nonlocal Kerr nonlinearity originated from the strong, long-range atom-atom interaction.

The dimensionless form of Eq. (5) reads

$$i \frac{\partial U}{\partial \zeta} + \frac{\partial^2 U}{\partial \xi^2} + \frac{\partial^2 U}{\partial \eta^2} - VU + \left( W_1 |U|^2 + \int \int d\xi' d\eta' W_2 (\xi' - \xi, \eta' - \eta) |U(\xi', \eta', \zeta)|^2 \right) U = 0, \quad (6)$$

where  $U = \Omega_p/U_0$ ,  $\zeta = z/z_0$ , and  $(\xi, \eta) = (x, y)/R_\perp$  [ $(\xi', \eta') = (x', y')/R_\perp$ ], with  $U_0$  the typical Rabi frequency of the probe beam,  $R_\perp$  the typical radius of the probe beam, and  $z_0 = 2k_p R_\perp^2 = 4\pi R_\perp^2/\lambda_p$  the characteristic diffraction distance. Here  $V = -k_p^2 R_\perp^2 \chi_p^{(1)}$  is an optical potential,  $W_1 = k_p^2 R_\perp^2 U_0^2 \chi_{p,1}^{(3)}$  characterizes the local Kerr nonlinearity, and  $W_2 = k_p^2 R_\perp^4 U_0^2 \tilde{\chi}_{p,2}^{(3)}$  characterizes the nonlocal Kerr nonlinearity.

### III. REALIZATION OF 2D $\mathcal{PT}$ -SYMMETRIC OPTICAL POTENTIAL AND ITS ACTIVE MANIPULATION

#### A. Realization of 2D $\mathcal{PT}$ -symmetric optical potential

We now turn to considering how to realize a linear 2D  $\mathcal{PT}$ -symmetric optical potential in the system. Since our system is highly manipulatable, it is viable to design different optical potentials  $V(\xi, \eta) = V_r(\xi, \eta) + iV_i(\xi, \eta)$ , which satisfy the condition of  $\mathcal{PT}$  symmetry, i.e.,  $V_r(-\xi, \eta) = V_r(\xi, \eta)$ ,  $V_r(\xi, -\eta) = V_r(\xi, \eta)$ ,  $V_i(-\xi, \eta) = -V_i(\xi, \eta)$ , and  $V_i(\xi, -\eta) = -V_i(\xi, \eta)$ . Here the subscripts  $r$  and  $i$  stand for their real and imaginary parts, respectively. By using the method of potential engineering proposed in Ref. [20], where 1D optical potential of  $\mathcal{PT}$  symmetry was realized, we can obtain various 2D  $\mathcal{PT}$ -symmetric optical potentials. Appendix B describes the detail of such a method for how to get a target 2D optical potential with  $\mathcal{PT}$  symmetry for the present system.

We assume that the target optical potential we hope to realize is a  $\mathcal{PT}$ -symmetric 2D period function with the form

$$V(\xi, \eta) = V_0 + V_1 [\sin^2(\xi) + \sin^2(\eta)] + iV_2 [\sin(2\xi) + \sin(2\eta)], \quad (7)$$

where  $V_0$  is a constant that contributes a constant phase factor for the probe beam;  $V_1$  and  $V_2$  ( $|V_1|, |V_2| \ll V_0$ ) are also constants but they characterize respectively the amplitudes of the real and imaginary parts of the periodic functions in the potential. Using the parameters of  $^{88}\text{Sr}$  atoms given in the previous section, the periodic potential (7) can be created by

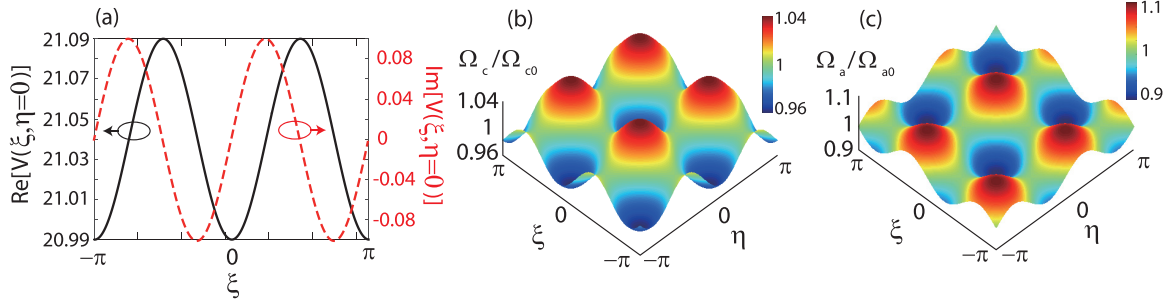


FIG. 2. Realization of the 2D  $\mathcal{PT}$ -symmetric optical potential. (a)  $\mathcal{PT}$ -symmetric optical potential (7) with  $(V_1, V_2) = (0.1, 0.1)$  of the Rydberg-dressed EIT system as a function of  $\xi = x/R_\perp$  at  $\eta = y/R_\perp = 0$ . The real part of optical potential  $\text{Re}(V)$  (black solid line) and the imaginary part of optical potential  $\text{Im}(V)$  (red dashed line) versus  $\xi$  are plotted. (b),(c) 2D spatial distributions of  $\Omega_c$  [panel (b)] and  $\Omega_a$  [panel (c)], required to obtain the  $\mathcal{PT}$ -symmetric period potential.

the following spatial modulation of the control and assistant fields:

$$\Omega_c(\xi)/\Omega_{c0} \approx 1 + 0.21V_2[\sin(2\xi) + \sin(2\eta)], \quad (8a)$$

$$\Omega_a(\xi)/\Omega_{a0} \approx 1 + 0.37\{V_1(\sin^2 \xi + \sin^2 \eta) - V_2[\sin(2\xi) + \sin(2\eta)]\}. \quad (8b)$$

When deriving (8), we have taken  $V_0 = 20.99$ . Note that the periodic spatial modulation of the control and assistant fields (8) can be realized experimentally by using high-resolution space-light modulators [44–46] with the pixel size smaller than the probe-beam radius  $R_\perp$ .

Turning to the nonlinear regime, we need to compute the coefficients for both the local and nonlocal nonlinearities by using the expression of  $W_1$  and  $W_2$  given in the last section. With the parameters of  $^{88}\text{Sr}$  atoms and choosing  $U_0 \approx 2.7 \times 10^6 \text{ s}^{-1}$ , we obtain  $W_1 \approx (1.4 + i7.8) \times 10^{-5}$  and  $W_2(\xi' - \xi, \eta' - \eta) \approx (0.19 - i0.27) \int dz \{1 - i2.4 + [(\xi' - \xi)^2 R_\perp^2 + (\eta' - \eta)^2 R_\perp^2 + z^2]/(0.6R_b)^6\}^{-1}$ , where  $R_b$  is the radius of the blockade sphere [47] (which is estimated to be  $9.46 \mu\text{m}$  in our system by the parameters given above),  $W_2$  obeys the normalization condition  $\int \int d\xi d\eta W_2(\xi, \eta) \approx 1$ , and the degree of the nonlocality is characterized by the parameter

$$\sigma \equiv 0.6R_b/R_\perp. \quad (9)$$

Note that the nonlocal nonlinearity in our system is four orders of magnitude larger than the local one, which allows us to keep only the nonlocal nonlinearity and neglect the local one. Furthermore, for  $^{88}\text{Sr}$  we have  $\text{Re}(W_2) > 0$ ; the optical interaction contributed by the nonlocal nonlinearity is attractive (focusing). This is because the dispersion parameter of the gas of  $^{88}\text{Sr}$  atoms is positive ( $C_6 > 0$ ). In principle, our approach is valid for any Rydberg gas. One can also obtain a repulsive (defocusing) nonlocal nonlinearity by using a different kind of atom (e.g.,  $^{87}\text{Rb}$  gas), which has a negative dispersion parameter (i.e.,  $C_6 < 0$ ).

Shown in Fig. 1(c) is spatial distributions of the real and imaginary parts of the nonlocal nonlinear coefficient  $W_2$ , i.e.,  $\text{Re}(W_2)$  and  $\text{Im}(W_2)$ , in the plane of dimensionless spatial coordinates  $\xi = x/R_\perp$  and  $\eta = y/R_\perp$ . The degree of the nonlocality is taken as  $\sigma = 0.6$  (i.e.,  $R_\perp = R_b$ ). The system parameters are the same with those used in Fig. 1(b). We see

that the maximum of  $\text{Im}(W_2)$  is approximately one order of magnitude smaller than that of  $\text{Re}(W_2)$ , and thus it can be neglected in the analytical research.

After dropping the constant part of the potential and neglecting the local nonlinearity (which is very small indicated above), Eq. (6) becomes the variable-coefficient nonlocal nonlinear Schrödinger equation (NNLSE)

$$i \frac{\partial U}{\partial \zeta} + \frac{\partial^2 U}{\partial \xi^2} + \frac{\partial^2 U}{\partial \eta^2} - V(\xi, \eta)U + \left( \iint d\xi' d\eta' W_2(\xi - \xi', \eta - \eta') |U(\xi', \eta', \zeta)|^2 \right) U = 0, \quad (10)$$

where  $V(\xi, \eta)$  is given by the  $\mathcal{PT}$ -symmetric potential (7). Since the degree of the nonlocality  $\sigma$  is proportional to the ratio  $R_b/R_\perp$ , one may tune  $\sigma$  by simply changing the probe-beam radius  $R_\perp$  if the blockade radius  $R_b$  is fixed. For a very large  $R_\perp$ ,  $\sigma$  is very small, the integral kernel  $W_2$  approaches into a  $\delta$  function, and hence the NNLSE (10) reduces into a local NLSE. In the opposite limit, i.e., for a very small  $R_\perp$ , the integral term in the NNLSE reduces into the form  $W_{20}P(\xi^2 + \eta^2)$  [see Eq. (11) below].

Shown in Fig. 2(a) is the  $\mathcal{PT}$ -symmetric optical potential  $V$  of the Rydberg-dressed EIT system as a function of  $\xi$  at  $\eta = 0$ , by taking  $V_1 = V_2 = 0.1$  and other parameters given above. The real part  $[\text{Re}(V)]$  and the imaginary part  $[\text{Im}(V)]$  of  $V$  are given by the black solid line and by the red dashed line, respectively. Figures 2(b) and 2(c) illustrate the 2D spatial distributions of the half Rabi frequencies of the control and assistant fields, i.e.,  $\Omega_c$  [panel (b)] and  $\Omega_a$  [panel (c)], which are required to satisfy the condition to obtain the  $\mathcal{PT}$ -symmetric period potential (7). In fact, we can also get any 2D optical potentials with  $\mathcal{PT}$  symmetry that are different from (7) by using the method of potential engineering described in Appendix B, which are omitted here for saving space.

## B. Active manipulation of the $\mathcal{PT}$ phase transition

One of key characters of a system of  $\mathcal{PT}$  symmetry is that the eigenvalue spectrum of the system displays a transition from real to complex when the ratio in the potential between the imaginary part of the potential and its real part is varied. In the linear limit, if this ratio is less than 0.5 the system possesses full  $\mathcal{PT}$  symmetry and the eigenvalue spectrum is

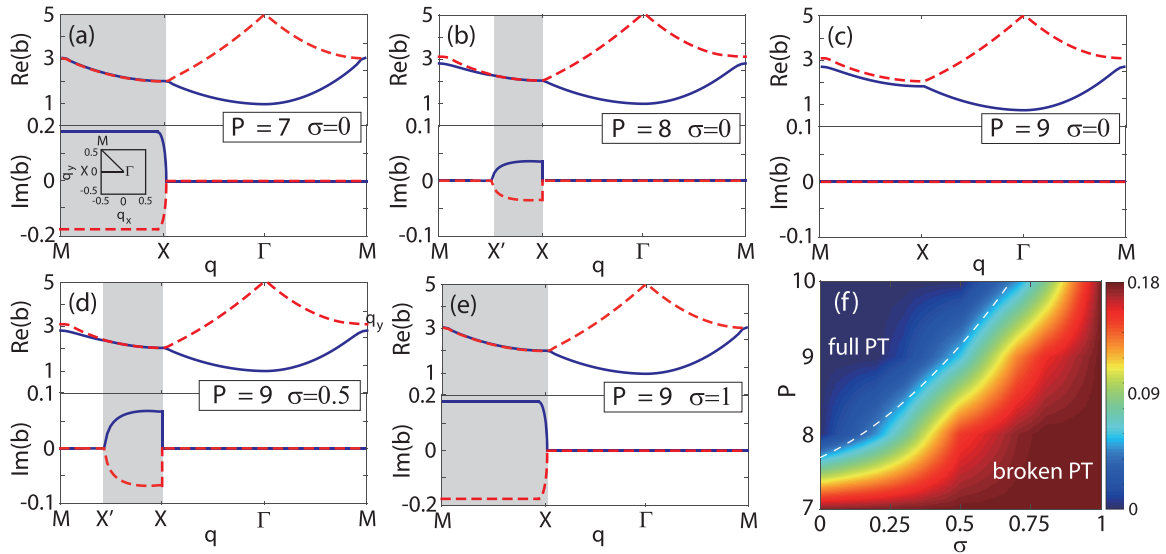


FIG. 3. Active manipulation of the  $\mathcal{PT}$  phase transition by the nonlocal optical nonlinearity. Shown in (a)–(e) are the real part  $\text{Re}(b)$  and the imaginary part  $\text{Im}(b)$  ( $b$  is propagation constant) as functions of the lattice momentum  $q = \sqrt{q_x^2 + q_y^2}$  for the  $\mathcal{PT}$ -symmetric potential (7), for different light power  $P$  and degree of the nonlocality  $\sigma$ , with  $(V_1, V_2) = (1, 0.6)$ . (a)  $\text{Re}(b)$  and  $\text{Im}(b)$  versus  $q$  along points  $M, X, \Gamma, M$  for  $(P, \sigma) = (7, 0)$ . (b)  $\text{Re}(b)$  and  $\text{Im}(b)$  for  $(P, \sigma) = (8, 0)$ . (c)  $\text{Re}(b)$  and  $\text{Im}(b)$  for  $(P, \sigma) = (9, 0)$ . (d)  $\text{Re}(b)$  and  $\text{Im}(b)$  for  $(P, \sigma) = (9, 0.5)$ . (e)  $\text{Re}(b)$  and  $\text{Im}(b)$  for  $(P, \sigma) = (9, 1)$ . Shaded domains in (a)–(e) indicate the region where the  $\mathcal{PT}$  symmetry is broken. (f) Phase diagram of the  $\mathcal{PT}$  symmetry in the plane of  $(\sigma, P)$ , determined by the maximum of  $\text{Im}(b)$ . The white dashed line represents the  $\mathcal{PT}$  phase transition. The system works in the full (broken)  $\mathcal{PT}$ -symmetric phase when  $\sigma$  is small (large) and  $P$  is large (small).

entirely real; if the ratio is larger than 0.5 the system works in the regime of broken  $\mathcal{PT}$  symmetry and the eigenvalue spectrum becomes complex.

However, the spectrum of nonlinear systems with linear  $\mathcal{PT}$  symmetry is less investigated up to now. A recent work [48] revealed that the inclusion of local Kerr nonlinearity can make the system transform from a broken (full)  $\mathcal{PT}$  symmetry to a full (broken) one if the Kerr nonlinearity is focusing (defocusing). However, how a nonlocal Kerr nonlinearity affects the physical behavior in systems with  $\mathcal{PT}$ -symmetry remains unexplored. We show below that the Kerr nonlinearity and its degree of nonlocality, contributed by the atom-atom interaction in Rydberg atoms, can be used to manipulate the  $\mathcal{PT}$  phase transition of the system.

The eigenvalue problem of linearized Eq. (6) is given by  $\hat{L}u = bu$ , where the Schrödinger operator  $\hat{L} \equiv \partial^2/\partial\xi^2 + \partial^2/\partial\eta^2 - V_1[\sin^2(\xi) + \sin^2(\eta)] - iV_2[\sin(2\xi) + \sin(2\eta)]$  and the propagation constant  $b$  is defined through the relation  $U(\xi, \eta) = e^{ibz}u(\xi, \eta)$ . Though a general discussion can be made for different  $V_1$  and  $V_2$ , here we focus only on a special case, i.e., the optical potential with  $(V_1, V_2) = (1, 0.6)$ . Since the ratio  $V_2/V_1 > 0.5$ , the system works in the regime with broken  $\mathcal{PT}$  symmetry in a linear limit.

We first discuss the influence of the Kerr nonlinearity on the  $\mathcal{PT}$  symmetry in the system, by taking the degree of the nonlocality  $\sigma$  [i.e., let  $R_\perp \gg R_b$ ; see Eq. (9)] to be zero (i.e., the nonlinearity of the system becomes a local one). Shown in Fig. 3(a) is the result of the eigenspectrum of the system. The real part  $\text{Re}(b)$  and the imaginary part  $\text{Im}(b)$  are illustrated as functions of the lattice momentum  $q = \sqrt{q_x^2 + q_y^2}$  for  $P = 5$  [here  $P \equiv \int_{-\infty}^{\infty} d\xi d\eta |U(\xi, \eta)|^2$  is dimensionless probe-field

light power], when  $q$  goes along points  $M, X, \Gamma$ , and  $M$ . From the figure, we see that two branches (plotted by the blue solid and red dashed lines, respectively) of  $\text{Re}(b)$  in the domain  $q \in [M, X]$  coalesce into one branch, when  $q$  goes across the  $X$  point from the right and enters the domain  $q \in [X, M]$ , where  $\text{Im}(b)$  becomes nonzero (or the eigenvalue  $b$  becomes complex). That is to say, the system is  $\mathcal{PT}$  symmetric in the domain  $q \in [X, M]$  (the white region in the figure), but the  $\mathcal{PT}$  symmetry is broken in the domain  $q \in [M, X]$  (the shaded region in the figure).

Figure 3(b) shows the result for  $(P, \sigma) = (8, 0)$ . In this case the Kerr nonlinearity is larger than that in Fig. 3(a). The system is  $\mathcal{PT}$  symmetric in the domain  $q \in [X, M]$  and  $q \in [M, X']$  (the white region in the figure), where  $\text{Im}(b)$  becomes zero. The shaded region ( $q \in [X', X]$ , where the  $\mathcal{PT}$  symmetry is broken) shrinks compared with Fig. 3(a). If increasing the Kerr nonlinearity further by taking  $P = 9$ , two branches of  $\text{Re}(b)$  are separated completely, and  $\text{Im}(b) = 0$  in the whole domain of  $q$  [see Fig. 3(c)]. Thus the system reenters a  $\mathcal{PT}$ -symmetric phase. From Figs. 3(a)–3(c), we conclude that by increasing the Kerr nonlinearity the system can be transformed from a broken  $\mathcal{PT}$  symmetry to a full  $\mathcal{PT}$  symmetry.

Then, we investigate the effect of the degree of the nonlocality of the Kerr nonlinearity on the  $\mathcal{PT}$  symmetry. For this aim, we fix  $P$  but take a nonzero  $\sigma$  of the system. Shown in Fig. 3(d) is the result of  $\text{Re}(b)$  and  $\text{Im}(b)$  versus  $q$  for  $(P, \sigma) = (9, 0.5)$ . Although the light power  $P$  is the same as in Fig. 3(c), the property of the  $\mathcal{PT}$  symmetry is quite different. In this case the system has no full  $\mathcal{PT}$  symmetry, i.e., a domain of broken  $\mathcal{PT}$ -symmetric phase [ $q \in [X', X]$ ; the shaded region in Fig. 3(d)] appears, again. Consequently,

the nonlocality of the Kerr nonlinearity can change the  $\mathcal{PT}$  symmetry of the system.

Figure 3(e) shows the result for a larger degree of the nonlocality by taking  $(P, \sigma) = (9, 1)$ . In this case, the  $q$  interval of the broken  $\mathcal{PT}$  symmetry phase (the shaded region) is enlarged compared with the one in the case of a smaller  $\sigma$  [Fig. 3(d)]. In particular, two branches of  $\text{Re}(b)$  coalesce into one in the domain of  $q \in [M, X]$  where  $\text{Im}(b)$  becomes nonzero.

To get a clear illustration of the property of the  $\mathcal{PT}$  symmetry in the system, a phase diagram is plotted [see Fig. 3(f)], which is determined by the maximum of  $\text{Im}(b)$ , for different light power  $P$  and the degree of the nonlocality of the Kerr nonlinearity  $\sigma$ . We see that the system works in the regime of full  $\mathcal{PT}$  symmetry when  $\sigma$  is small and  $P$  is large (the domain with blue color), while it works in the regime of broken  $\mathcal{PT}$  symmetry when  $\sigma$  is large and  $P$  is small (the domain with red color). The white dashed curve in the figure represents roughly the position where  $\mathcal{PT}$  phase transition occurs in the  $(\sigma, P)$  phase plane.

To understand the effect of the degree of nonlocality on the character of the  $\mathcal{PT}$  phase transition in the system, we take a special case of strongly nonlocal regime (i.e.,  $\sigma \gg 1$ ), in which the NNLSE (10) can be reduced into the simple form

$$i \frac{\partial U}{\partial \xi} + \frac{\partial^2 U}{\partial \xi^2} + \frac{\partial^2 U}{\partial \eta^2} - V(\xi, \eta)U + W_{20}P(\xi^2 + \eta^2)U = 0, \quad (11)$$

with  $W_{20} = W_2(\xi = 0, \eta = 0)$ , which means that the nonlocal Kerr nonlinearity in the NNLSE (10) has been reduced into an effective parabolic potential [49] [i.e., the last term on the right-hand side of Eq. (11)]. The physical reason for this reduction is that all the photons in the probe beam experience a similar potential due to the very narrow beam radius and the very wide spatial distribution of the Kerr nonlinearity. As a result, we obtain a new  $\mathcal{PT}$ -symmetric optical potential, given by  $V_{\text{tot}} = V(\xi, \eta) - W_{20}P(\xi^2 + \eta^2)$ , where  $W_{20} > 0$  for the focusing nonlinearity. Obviously, the new optical potential  $V_{\text{tot}}$  has different ratio between the imaginary part and the real part, in contrast with the case having only the optical potential  $V(\xi, \eta)$ . Consequently, the character of the  $\mathcal{PT}$  symmetry in the system is changed by the nonlocal Kerr nonlinearity via the atom-atom interaction inherent in Rydberg atoms.

#### IV. NONLOCAL OPTICAL SOLITONS AND THEIR ACTIVE CONTROL

Compared to conventional nonlinear optical media, the present Rydberg atomic system has an additional tunable parameter, i.e., the degree of the nonlocality of the Kerr nonlinearity (9), to manipulate the  $\mathcal{PT}$  symmetry, as shown in the last section. In this section, we shall demonstrate that not only stable nonlocal optical solitons exist in the system, but also the degree of the nonlocality may be used to actively control the behavior of these solitons.

First, we discuss possible nonlocal optical solitons in the system. By using a method of imaginary time evolution, we find that a 2D nonlocal optical gap soliton for  $C_6 < 0$

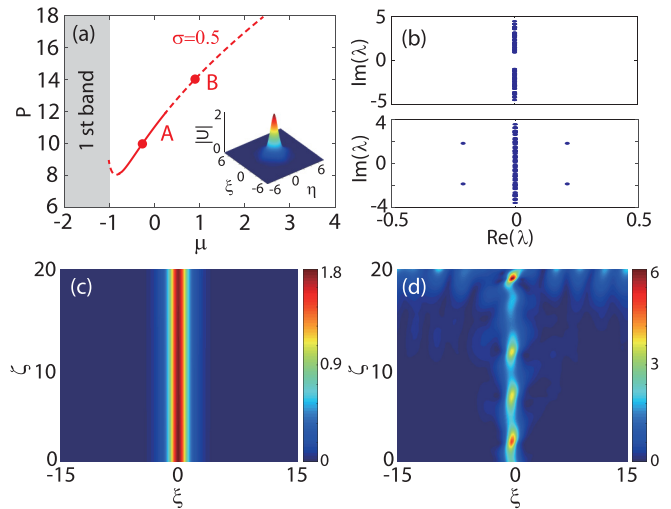


FIG. 4. Nonlocal optical gap solitons and their stability. (a) Curve of  $P$ - $\mu$  ( $\mu \equiv -b$ ;  $b$  is propagation constant) for degree of nonlocality  $\sigma = 0.5$  and the optical potential parameters  $(V_1, V_2) = (1, 0.3)$ . Nonlocal gap solitons exist in some regions of the semi-infinite gap [i.e., in the region  $\mu > -1$ ; the shaded region ( $\mu < -1$ ) is the first energy band]. Solid part (where point “A” locates) and dashed part (where point “B” locates) in the red curve represent stable and unstable regions of nonlocal gap solitons, respectively. Inset: dimensionless wave shape  $|U| = |\Omega_p/U_0|$  for a typical 2D nonlocal optical soliton with  $P = 10$ . (b) Stability spectrum for small perturbations around the optical gap soliton with  $P = 10$  (upper panel) and with  $P = 14$  (lower panel).  $\text{Re}(\lambda)$  and  $\text{Im}(\lambda)$  are real part and imaginary part of the eigenvalue  $\lambda$  of the small perturbations, respectively. (c),(d) Propagation of the nonlocal gap soliton under small perturbations as functions of  $\xi = x/R_\perp$  and  $\zeta = z/z_0$ , for  $P = 10$  [panel (c)] and  $P = 14$  [panel (d)]. The soliton propagates robustly against the perturbations in the  $\mathcal{PT}$ -symmetry phase [panel (c)], but it breaks up in the broken  $\mathcal{PT}$ -symmetry phase [panel (d)].

(i.e., self-focusing nonlocal Kerr nonlinearity) of the NNLSE (10) can be obtained, with the dimensionless wave shape  $|u| = |\Omega_p/U_0|$  given in the inset of Fig. 4(a), where the light power  $P = 10$  (corresponding to the point “A” in the figure) and other parameters the same as before. To give a general picture for the existence and stability of the soliton, the light power  $P$  as a function of  $\mu$  ( $\mu = -b$ ;  $b$  is the propagation constant) is plotted for the degree of the nonlocality  $\sigma = 0.5$  and the optical potential (7) with  $(V_1, V_2) = (1, 0.3)$ . The soliton exists only in some regions of the semi-infinite gap [i.e., the region  $\mu > -1$ ; the shaded region (the one  $\mu < -1$ ) is the first energy band]. The solid-line part (where point A locates) and dashed-line part (where point “B” locates) in the red curve represent stable and unstable regions of nonlocal gap solitons, respectively.

The maximum intensity of the nonlocal optical gap soliton with  $P = 10$  (the point marked by A) in Fig. 4(a) can be estimated by using the formula  $I_{\text{max}} = c\epsilon_0 |\mathbf{E}_{p,\text{max}}|^2/2$ . We obtain that  $I_{\text{max}} \approx 5.4 \times 10^{-5} \text{ W cm}^{-2}$  based on the parameters of  $^{88}\text{Sr}$  atoms provided above. Thus, to produce a nonlocal gap soliton, only a very low input light intensity is needed. We remark that the generation power of a single 800 nm photon per microsecond is  $I_{\text{ph}} \approx 2.5 \times 10^{-11} \text{ W cm}^{-2}$ . This

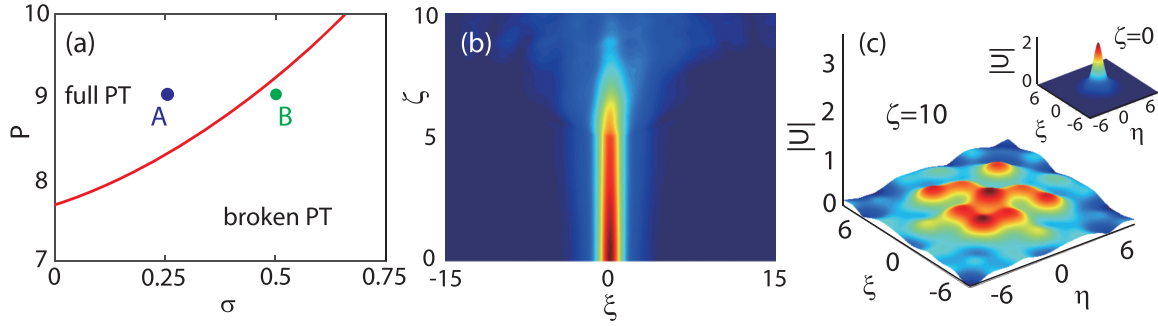


FIG. 5. Active control of the nonlocal gap solitons. (a)  $\mathcal{PT}$  phase diagram in the plane of  $(P, \sigma)$  for the optical potential (7) with  $(V_1, V_2) = (1, 0.6)$ . The red solid line represents the  $\mathcal{PT}$  phase transition, above (below) which is the region of full (broken)  $\mathcal{PT}$  symmetry. A nonlocal gap soliton with light power  $P = 9$  and the degree of the nonlocality  $\sigma = 0.25$  (marked by the point “A”) is stable; however, a nonlocal gap soliton with the same light power but  $\sigma = 0.5$  (marked by the point “B”) is unstable. (b) Propagation of the nonlocal gap soliton (as functions of  $\xi = x/R_{\perp}$  and  $\zeta = z/z_0$ ) by changing the value of  $\sigma$  during the propagation. The soliton loses its stability at  $\zeta \approx 5$ , where  $\sigma$  is increased rapidly from 0.25 to 0.5. (c) Dimensionless amplitude of the output soliton  $|u| = |\Omega_p/U_0|$  at  $\zeta = 10$ , where a significant deformation and attenuation occurs. Dimensionless amplitude of the input soliton at  $\zeta = 0$  cm is also given, as shown in the inset.

indicates that a typical nonlocal gap soliton formed in our system contains only millions of photons. This is in a sharp contrast with cases of nonresonant media, where much higher input intensity and much longer optical path are necessary and required for the formation of optical solitons.

Second, we carry out a linear stability analysis to understand the stability property of the nonlocal gap solitons described above. We take  $U(\zeta, \xi, \eta) = e^{-i\mu\zeta} [u(\xi, \eta) + \tilde{v}(\xi, \eta)e^{\lambda\zeta} + \tilde{w}^*(\xi, \eta)e^{\lambda^*\zeta}]$ , where  $u$  represents a soliton,  $\tilde{v}$  and  $\tilde{w}$  are small perturbations to the soliton, and  $\lambda$  is the eigenvalue of the perturbations. Based on Eq. (10) we get the eigenvalue problem for the perturbations

$$\lambda \tilde{v} = i \left( \mu + \frac{\partial^2}{\partial \xi^2} + \frac{\partial^2}{\partial \eta^2} + V(\xi, \eta) + n \right) \tilde{v} + iu \Delta n, \quad (12a)$$

$$\lambda \tilde{w} = -i \left( \mu + \frac{\partial^2}{\partial \xi^2} + \frac{\partial^2}{\partial \eta^2} + V^*(\xi, \eta) + n \right) \tilde{w} - iu^* \Delta n, \quad (12b)$$

where  $n = \iint d\xi' d\eta' W_2(\xi - \xi', \eta - \eta') |u(\xi', \eta')|^2$  and  $\Delta n = \iint d\xi' d\eta' W_2(\xi - \xi', \eta - \eta') u^*(\xi', \eta') \tilde{v}(\xi', \eta') + \iint d\xi' d\eta' W_2(\xi - \xi', \eta - \eta') u(\xi', \eta') \tilde{w}(\xi', \eta')$ . If the eigenvalue is found to have a positive real part, the soliton is unstable; otherwise, it is stable.

The eigenvalue problem (12) is numerically computed by using the Fourier collocation method [50]. Due to the gain-loss component in the optical potential ( $V_2 > 0$ ), the soliton is stable in a finite  $\mu$  interval [i.e., the red solid-line part in Fig. 4(a)]; unstable regions appear close to the border of the semi-infinite gap where  $\partial P/\partial \mu < 0$  and for larger values of  $\mu$  [i.e., red dashed-line parts in Fig. 4(a)].

In Fig. 4(b) we show the stability spectrum for the perturbations respective to the soliton with  $P = 10$  [upper panel, corresponding to the point A in Fig. 4(a)] and to the soliton with  $P = 14$  [lower panel, corresponding to the point B in Fig. 4(a)], where  $\text{Re}(\lambda)$  and  $\text{Im}(\lambda)$  are respectively real part and imaginary part of the eigenvalue  $\lambda$  of the perturbations. The soliton corresponding to the point A is stable since

$\text{Im}(\lambda) = 0$ , whereas the soliton corresponding to the point B is unstable since a quadruple of complex  $\lambda$  appears. Illustrated in Fig. 4(c) [Fig. 4(d)] is propagation of the soliton corresponding to the upper (lower) panel of Fig. 4(b) under perturbations, as functions of  $\xi = x/R_{\perp}$  and  $\zeta = z/z_0$ . We see that the soliton corresponding to the upper (lower) panel is indeed stable (unstable) against the perturbations during propagation.

Third, we demonstrate that the degree of the nonlocality of the Kerr nonlinearity  $\sigma$ , which is tunable in our system by changing the radius of the blockade sphere beam or the radius of the probe beam, can be used to control the behavior of nonlocal gap solitons. In Fig. 5(a) we show the  $\mathcal{PT}$  phase diagram in the plane of  $(P, \sigma)$  in the optical potential (7) with  $(V_1, V_2) = (1, 0.6)$ . The red solid line in the figure represents the  $\mathcal{PT}$  phase transition, above (below) which is the region of full (broken)  $\mathcal{PT}$  symmetry. We find that the nonlocal gap soliton with light power  $P = 9$  and  $\sigma = 0.25$  (marked by the point A) is stable; however, by tuning the degree of the nonlocality to the value  $\sigma = 0.5$ , the soliton with the same light power (marked by the point B) becomes unstable.

We have also investigated the behavior of the nonlocal gap soliton by adjusting  $\sigma$  during the propagation of the soliton (as functions of  $\xi = x/R_{\perp}$  and  $\zeta = z/z_0$ ), with the result plotted in Fig. 5(b). We see that the soliton loses its stability immediately at the position  $\zeta \approx 5$  where  $\sigma$  is increased from 0.25 to 0.5 rapidly. Figure 5(c) shows a 3D plot of the output soliton at the distance  $\zeta = 10$ . One can see that the dimensionless amplitude  $|u| = |\Omega_p/U_0|$  of the soliton displays a significant deformation and attenuation, although its input (at  $\zeta = 0$ ) is a soliton with a nice shape (see the inset of the figure).

Note that the approach presented above can also be applied to the system with defocusing nonlocal Kerr nonlinearity, which is the case of, e.g., the rubidium atoms excited to the Rydberg state. In this situation, because  $C_6 > 0$ , the parameter  $W_{20}$  in the total optical potential  $V_{\text{tot}}$  contributed by the atom-atom interaction will become negative. As a result, nonlocal gap solitons obtained can be more stable when the degree of the nonlocality of the Kerr nonlinearity  $\sigma$  is increased.

## V. SUMMARY

In this work, we have proposed a scheme for realizing  $\mathcal{PT}$  symmetry and nonlocal high-dimensional optical gap solitons via a Rydberg-dressed EIT. We have shown that a 2D complex optical potential with a periodic  $\mathcal{PT}$  symmetry for the probe-field propagation can be obtained when the incoherent population pumping between two low-lying states is employed and the spatial modulations of the control and assisted laser fields is engineered. We have also shown that, based on the giant nonlocal Kerr nonlinearity, originated from the strong, long-range interaction between Rydberg atoms, the system supports nonlocal (2+1)-dimensional spatial gap solitons, which have very low light intensity. In particular, we have found that the Kerr nonlinearity and its degree of nonlocality, which can be actively tuned in our system,

have apparent effects on the phase transition of the  $\mathcal{PT}$  symmetry and the behavior of the nonlocal optical solitons. The research presented here opens a route for developing non-Hermitian nonlinear optics, in particular for manipulating the optical solitons with controllable  $\mathcal{PT}$ -symmetric optical potential and nonlocal Kerr nonlinearity, which may find applications in optical information processing and transmission.

## ACKNOWLEDGMENTS

The authors thank Weibin Li for useful discussions. This work was supported by the National Natural Science Foundation of China under Grants No. 11475063 and No. 11474099 and by the National Basic Research Program of China under Grant No. 2016YFA0302103.

## APPENDIX A: EXPANSION EQUATIONS OF DENSITY-MATRIX ELEMENTS AND THEIR SOLUTIONS

(i) At the zeroth ( $m = 0$ ) order, equations for  $\rho_{32}^{(0)}$ ,  $\rho_{42}^{(0)}$ , and  $\rho_{43}^{(0)}$  are given by

$$\begin{pmatrix} d_{32} & \Omega_c^* & 0 \\ \Omega_c & d_{42} & -\Omega_a \\ 0 & -\Omega_a^* & d_{43} \end{pmatrix} \begin{pmatrix} \rho_{32}^{(0)} \\ \rho_{42}^{(0)} \\ \rho_{43}^{(0)} \end{pmatrix} = \begin{pmatrix} \Omega_a(\rho_{33}^{(0)} - \rho_{22}^{(0)}) \\ 0 \\ -\Omega_c \rho_{33}^{(0)} \end{pmatrix}. \quad (\text{A1})$$

Equations for  $\rho_{11}^{(0)}$ ,  $\rho_{22}^{(0)}$ , and  $\rho_{33}^{(0)}$  read

$$\begin{pmatrix} -\Gamma_{21} & 0 & \Gamma_{13} \\ \Gamma_{21} & 0 & \Gamma_{23} \\ 1 & 1 & 1 \end{pmatrix} \begin{pmatrix} \rho_{11}^{(0)} \\ \rho_{22}^{(0)} \\ \rho_{33}^{(0)} \end{pmatrix} = \begin{pmatrix} 0 \\ 2 \text{Im}(\Omega_a^* \rho_{32}^{(0)}) \\ 1 \end{pmatrix}. \quad (\text{A2})$$

The solution reads

$$\rho_{11}^{(0)} = -\Gamma_{13}X/[\Gamma_{21}\Gamma_{13} - (\Gamma_{21} + \Gamma_{13})X + \Gamma_{21}(\Gamma_{23} + Y)], \quad (\text{A3a})$$

$$\rho_{22}^{(0)} = \Gamma_{21}(\Gamma_{13} + \Gamma_{23} + Y)/[\Gamma_{21}\Gamma_{13} - (\Gamma_{21} + \Gamma_{13})X + \Gamma_{21}(\Gamma_{23} + Y)], \quad (\text{A3b})$$

$$\rho_{33}^{(0)} = -\Gamma_{21}X/[\Gamma_{21}\Gamma_{13} - (\Gamma_{21} + \Gamma_{13})X + \Gamma_{21}(\Gamma_{23} + Y)], \quad (\text{A3c})$$

$$\rho_{32}^{(0)} = [-(d_{42}d_{43} - |\Omega_c|^2)\rho_{22}^{(0)} + (d_{42}d_{43} - |\Omega_c|^2 + |\Omega_a|^2)\rho_{33}^{(0)}]\Omega_c/D_1, \quad (\text{A3d})$$

$$\rho_{42}^{(0)} = [d_{43}\rho_{22}^{(0)} - (d_{32} + d_{43})\rho_{33}^{(0)}]\Omega_c\Omega_a/D_1, \quad (\text{A3e})$$

$$\rho_{43}^{(0)} = [|\Omega_c|^2\rho_{22}^{(0)} - (d_{32}d_{42} + |\Omega_c|^2 - |\Omega_a|^2)\rho_{33}^{(0)}]\Omega_a/D_1, \quad (\text{A3f})$$

$$\rho_{21}^{(0)} = \rho_{31}^{(0)} = \rho_{41}^{(0)} = \rho_{44}^{(0)} = 0, \quad (\text{A3g})$$

where  $X = 2 \text{Im}[(d_{42}d_{43} - |\Omega_c|^2)|\Omega_c|^2/D_1]$  and  $Y = -2 \text{Im}[(d_{42}d_{43} - |\Omega_c|^2 + |\Omega_a|^2)|\Omega_c|^2/D_1]$ ,  $\rho_{44}^{(0)} = 1 - \sum_{j=1}^3 \rho_{jj}^{(0)}$ , with  $D_1 = d_{32}d_{42}d_{43} - |\Omega_c|^2d_{32} - |\Omega_a|^2d_{43}$ .

(ii) At the first ( $m = 1$ ) order, the solution for nonzero matrix elements reads  $\rho_{21}^{(1)} = \alpha_{21}^{(1)}\Omega_p$ ,  $\rho_{31}^{(1)} = \alpha_{31}^{(1)}\Omega_p$ ,  $\rho_{41}^{(1)} = \alpha_{41}^{(1)}\Omega_p$ , where  $\alpha_{21}^{(1)}$ ,  $\alpha_{31}^{(1)}$ ,  $\alpha_{41}^{(1)}$  are determined by the equation

$$\begin{pmatrix} d_{21} & \Omega_a^* & 0 \\ \Omega_a & d_{31} & \Omega_c^* \\ 0 & \Omega_c & d_{41} \end{pmatrix} \begin{pmatrix} \alpha_{21}^{(1)} \\ \alpha_{31}^{(1)} \\ \alpha_{41}^{(1)} \end{pmatrix} = \begin{pmatrix} \rho_{23}^{(0)} \\ \rho_{33}^{(0)} - \rho_{11}^{(0)} \\ \rho_{43}^{(0)} \end{pmatrix}. \quad (\text{A4})$$

(iii) At the second ( $m = 2$ ) order, the solution for nonzero matrix elements is found to be  $\rho_{32}^{(2)} = \alpha_{32}^{(2)} |\Omega_p|^2$ ,  $\rho_{42}^{(2)} = \alpha_{42}^{(2)} |\Omega_p|^2$ ,  $\rho_{43}^{(2)} = \alpha_{43}^{(2)} |\Omega_p|^2$ ,  $\rho_{jj}^{(2)} = \alpha_{jj}^{(2)} |\Omega_p|^2$  ( $j = 1, 2, 3, 4$ ), with  $\alpha_{32}^{(2)}$ ,  $\alpha_{42}^{(2)}$ ,  $\alpha_{43}^{(2)}$  satisfying the equation

$$\begin{pmatrix} d_{32} & \Omega_c^* & 0 \\ \Omega_c & d_{42} & -\Omega_a \\ 0 & -\Omega_2^* & d_{43} \end{pmatrix} \begin{pmatrix} \alpha_{32}^{(2)} \\ \alpha_{42}^{(2)} \\ \alpha_{43}^{(2)} \end{pmatrix} = \begin{pmatrix} \Omega_a(\alpha_{33}^{(2)} - \alpha_{22}^{(2)}) - \alpha_{12}^{(1)} \\ 0 \\ \Omega_c(\alpha_{44}^{(2)} - \alpha_{33}^{(2)}) + \alpha_{41}^{(1)} \end{pmatrix}, \quad (\text{A5})$$

and  $\alpha_{jj}^{(2)}$  satisfying the equation

$$\begin{pmatrix} -\Gamma_{21} & 0 & \Gamma_{13} & 0 \\ \Gamma_{21} & 0 & \Gamma_{23} & 0 \\ 0 & 0 & -\Gamma_{13} - \Gamma_{23} & \Gamma_{34} \\ 1 & 1 & 1 & 1 \end{pmatrix} \begin{pmatrix} \alpha_{11}^{(2)} \\ \alpha_{22}^{(2)} \\ \alpha_{33}^{(2)} \\ \alpha_{44}^{(2)} \end{pmatrix} = \begin{pmatrix} 2 \text{Im}(\alpha_{31}^{(1)}) \\ 2 \text{Im}(\Omega_a^* \alpha_{32}^{(2)}) \\ 2 \text{Im}(\alpha_{31}^{(1)*} + \Omega_a \alpha_{32}^{(2)*} + \Omega_c^* \alpha_{43}^{(2)}) \\ 0 \end{pmatrix}. \quad (\text{A6})$$

(iv) At the third ( $m = 3$ ) order, the solution of  $\rho_{j1}^{(3)}$  ( $j = 1-3$ ) can be obtained from the equation

$$\begin{pmatrix} d_{21} & \Omega_a^* & 0 \\ \Omega_a & d_{31} & \Omega_c^* \\ 0 & \Omega_c & d_{41} \end{pmatrix} \begin{pmatrix} \rho_{21}^{(3)} \\ \rho_{31}^{(3)} \\ \rho_{41}^{(3)} \end{pmatrix} = \begin{pmatrix} \alpha_{23}^{(2)} \\ \alpha_{33}^{(2)} - \alpha_{11}^{(2)} \\ \alpha_{43}^{(2)} \end{pmatrix} |\Omega_p|^2 \Omega_p + \begin{pmatrix} 0 \\ 0 \\ \mathcal{N}_\alpha \int \mathbf{r}' V(\mathbf{r}' - \mathbf{r}) \alpha_{41}^{(1)*} \alpha_{4141}^{(2)} |\Omega_p(\mathbf{r}')|^2 \Omega_p(\mathbf{r}) \end{pmatrix}, \quad (\text{A7})$$

where  $\alpha_{4141}^{(2)}$  can be obtained from the equation

$$\begin{pmatrix} d_{21} & 0 & 0 & \Omega_a^* & 0 & 0 \\ 0 & d_{31} & 0 & \Omega_a & 0 & \Omega_c^* \\ 0 & 0 & d_{41} - V/2 & 0 & 0 & \Omega_c \\ \Omega_a & \Omega_a^* & 0 & d_{21} + d_{31} & \Omega_c^* & 0 \\ 0 & 0 & 0 & \Omega_c & d_{21} + d_{41} & \Omega_a^* \\ 0 & \Omega_c & \Omega_c^* & 0 & \Omega_a & d_{31} + d_{41} \end{pmatrix} \begin{pmatrix} \alpha_{2121}^{(2)} \\ \alpha_{3131}^{(2)} \\ \alpha_{4141}^{(2)} \\ \alpha_{2131}^{(2)} \\ \alpha_{2141}^{(2)} \\ \alpha_{3141}^{(2)} \end{pmatrix} = \begin{pmatrix} \rho_{23}^{(0)} \alpha_{21}^{(1)} \\ (\rho_{33}^{(0)} - \rho_{11}^{(0)}) \alpha_{31}^{(1)} \\ \rho_{43}^{(0)} \alpha_{41}^{(1)} \\ (\rho_{33}^{(0)} - \rho_{11}^{(0)}) \alpha_{21}^{(1)} + \rho_{23}^{(0)} \alpha_{31}^{(1)} \\ \rho_{23}^{(0)} \alpha_{41}^{(1)} + \rho_{43}^{(0)} \alpha_{21}^{(1)} \\ (\rho_{33}^{(0)} - \rho_{11}^{(0)}) \alpha_{41}^{(1)} + \rho_{43}^{(0)} \alpha_{31}^{(1)} \end{pmatrix}. \quad (\text{A8})$$

(v) Expressions of  $\alpha_{21}^{(1)}$ ,  $\alpha_{31}^{(1)}$ , and  $\alpha_{41}^{(1)}$  at the first order are obtained from Eq. (A4),

$$\alpha_{21}^{(1)} = [(d_{31}d_{41} - |\Omega_a|^2)\rho_{23}^{(0)} + \Omega_c^* \Omega_a^* \rho_{43}^{(0)} - d_{41} \Omega_c^* (\rho_{33}^{(0)} - \rho_{11}^{(0)})] / D_2, \quad (\text{A9a})$$

$$\alpha_{31}^{(1)} = [d_{21}d_{41}(\rho_{33}^{(0)} - \rho_{11}^{(0)}) - d_{41} \Omega_c \rho_{23}^{(0)} - d_{21} \Omega_a^* \rho_{43}^{(0)}] / D_2, \quad (\text{A9b})$$

$$\alpha_{41}^{(1)} = [(d_{21}d_{31} - |\Omega_c|^2)\rho_{43}^{(0)} + \Omega_c \Omega_a \rho_{23}^{(0)} - d_{21} \Omega_a (\rho_{33}^{(0)} - \rho_{11}^{(0)})] / D_2, \quad (\text{A9c})$$

where  $D_2 = d_{21}d_{31}d_{41} - |\Omega_c|^2 d_{41} - |\Omega_a|^2 d_{21}$ . Expressions of  $\alpha_{32}^{(2)}$ ,  $\alpha_{42}^{(2)}$ ,  $\alpha_{43}^{(2)}$ , and  $\alpha_{jj}^{(2)}$  at the second order can be obtained from Eq. (A5) and Eq. (A6). However, they are very lengthy and hence are omitted.

## APPENDIX B: DESIGN OF $\mathcal{PT}$ -SYMMETRIC OPTICAL POTENTIAL

The method of potential engineering proposed in Ref. [20] can be exploited to get various 2D  $\mathcal{PT}$ -symmetric optical potentials for the present system, with steps given in the following.

First, we note that the optical potential with  $\mathcal{PT}$  symmetry must satisfy the real condition at the origin  $\xi = \eta = 0$ , i.e.,  $V_i(\xi = 0, \eta = 0) = 0$ . To get a  $\mathcal{PT}$ -symmetric potential that has balanced gain and loss in the whole space, we assume that the Rabi frequencies of the control and assisted field are space dependent,  $\Omega_c = \Omega_c(\xi, \eta)$  and  $\Omega_a = \Omega_a(\xi, \eta)$ . Thus, if  $\Omega_c = \Omega_{c0}$  and  $\Omega_a = \Omega_{a0}$  at  $(\xi, \eta) = (0, 0)$ , the value of  $\Delta_3$  can be determined by solving the equation  $V_i(\Omega_{c0}, \Omega_{a0}, \Delta_3) = 0$ , referred to as  $\Delta_3 = \Delta_{30}$ , and hence the values of  $\Delta_2$  and  $\Delta_4$  can also be determined.

Next, we expand  $V_r$  and  $V_i$  around  $\Omega_c = \Omega_{c0}$  and  $\Omega_a = \Omega_{a0}$ , i.e.,

$$V_r(\Omega_c, \Omega_a, \Delta_{30}) = V_r(\Omega_{c0}, \Omega_{a0}, \Delta_{30}) + R_{1,0}(\Omega_c - \Omega_{c0}) + R_{0,1}(\Omega_a - \Omega_{a0}), \quad (\text{B1a})$$

$$V_i(\Omega_c, \Omega_a, \Delta_{30}) = I_{1,0}(\Omega_c - \Omega_{c0}) + I_{0,1}(\Omega_a - \Omega_{a0}), \quad (\text{B1b})$$

where

$$R_{m,n} = \frac{\partial^{m+n}}{\partial^m \Omega_c \partial^n \Omega_a} V_r(\Omega_c, \Omega_a, \Delta_{30})|_{\Omega_c=\Omega_{c0}, \Omega_a=\Omega_{a0}},$$

$$I_{m,n} = \frac{\partial^{m+n}}{\partial^m \Omega_c \partial^n \Omega_a} V_i(\Omega_c, \Omega_a, \Delta_{30})|_{\Omega_c=\Omega_{c0}, \Omega_a=\Omega_{a0}}.$$

Note that we have truncated the expansions by neglecting high-order terms, which means that  $\Omega_c$  and  $\Omega_a$  are taken as weakly space dependent.

Finally, in order to determine the profiles of  $\Omega_c(\xi, \eta)$  and  $\Omega_a(\xi, \eta)$ , we solve the following equation:

$$R_{1,0}(\Omega_c - \Omega_{c0}) + R_{0,1}(\Omega_a - \Omega_{a0}) = V_{\text{Tr}}(\xi, \eta) - V_r(\Omega_{c0}, \Omega_{a0}, \Delta_{30}), \quad (\text{B3a})$$

$$I_{1,0}(\Omega_c - \Omega_{c0}) + I_{0,1}(\Omega_a - \Omega_{a0}) = V_{\text{Ti}}(\xi, \eta), \quad (\text{B3b})$$

where  $V_T(\xi, \eta)$  denotes the target potential, which possesses  $\mathcal{PT}$  symmetry. If Eq. (B3) can be solved, the  $\mathcal{PT}$ -symmetric potential will be obtained successfully.

Note that the potential engineering method described above provides an accurate  $\mathcal{PT}$  symmetry only for small  $\xi$ . This imposes a constraint on the choice of the width of the probe beam, which should be small enough so that the undesirable deviation from the  $\mathcal{PT}$  symmetry at large  $\xi$  can be avoided.

- 
- [1] S. Boettcher and C. M. Bender, Real Spectra in Non-Hermitian Hamiltonians Having PT Symmetry, *Phys. Rev. Lett.* **80**, 5243 (1998).
- [2] A. Mostafazadeh, Exact PT symmetry is equivalent to Hermiticity, *J. Math. Phys.* **36**, 7081 (2003).
- [3] C. M. Bender, Making sense of non-Hermitian Hamiltonians, *Rep. Prog. Phys.* **70**, 947 (2007).
- [4] V. V. Konotop, J. Yang, and D. A. Zezyulin, Nonlinear waves in PT-symmetric systems, *Rev. Mod. Phys.* **88**, 035002 (2016).
- [5] L. Feng, R. El-Ganainy, and L. Ge, Non-Hermitian photonics based on parity-time symmetry, *Nat. Photon.* **11**, 752 (2017).
- [6] R. El-Ganainy, K. G. Makris, M. Khajavikhan, Z. H. Musslimani, S. Rotter, and D. N. Christodoulides, Non-Hermitian physics and PT symmetry, *Nat. Phys.* **14**, 11 (2018).
- [7] H. Ramezani, T. Kottos, R. El-Ganainy, and D. N. Christodoulides, Unidirectional nonlinear PT-symmetric optical structures, *Phys. Rev. A* **82**, 043803 (2010).
- [8] L. Feng, M. Ayache, J. Huang, Y.-L. Xu, M.-H. Lu, Y.-F. Chen, Y. Fainman, and A. Scherer, Nonreciprocal light propagation in a silicon photonic circuit, *Science* **333**, 729 (2011).
- [9] Z. Lin, H. Ramezani, T. Eichelkraut, T. Kottos, H. Cao, and D. Christodoulides, Unidirectional Invisibility Induced by PT-Symmetric Periodic Structures, *Phys. Rev. Lett.* **106**, 213901 (2011).
- [10] S. Longhi, PT-symmetric laser absorber, *Phys. Rev. A* **82**, 031801(R) (2010).
- [11] Y. D. Chong, L. Ge, and A. D. Stone, PT-Symmetry Breaking and Laser-Absorber Modes in Optical Scattering Systems, *Phys. Rev. Lett.* **106**, 093902 (2011).
- [12] Y. Sun, W. Tan, H. Li, J. Li, and H. Chen, Experimental Demonstration of a Coherent Perfect Absorber with PT Phase Transition, *Phys. Rev. Lett.* **112**, 143903 (2014).
- [13] V. V. Konotop, V. S. Shchesnovich, and D. A. Zezyulin, Giant amplification of modes in parity-time symmetric waveguides, *Phys. Lett. A* **376**, 2750 (2012).
- [14] L. Feng, Z. J. Wong, R. Ma, Y. Wang, and X. Zhang, Single mode laser by parity-time symmetry breaking, *Science* **346**, 972 (2014).
- [15] H. Hodaei, M.-A. Miri, M. Heinrich, D. N. Christodoulides, and M. Khajavikhan, Parity-time-symmetric microring lasers, *Science* **346**, 975 (2014).
- [16] H. Hodaei, A. U. Hassan, S. Wittek, H. Garcia-Gracia, R. El-Ganainy, D. N. Christodoulides, and M. Khajavikhan, Enhanced sensitivity at higher-order exceptional points, *Nature (London)* **548**, 187 (2017).
- [17] W. Chen, Ş. K. Özdemir, G. Zhao, J. Wiersig, and L. Yang, Exceptional points enhance sensing in an optical microcavity, *Nature (London)* **548**, 192 (2017).
- [18] L. Xiao, X. Zhan, Z. H. Bian, K. K. Wang, X. Zhang, X. P. Wang, J. Li, K. Mochizuki, D. Kim, N. Kawakami, W. Yi, H. Obuse, B. C. Sanders, and P. Xue, Observation of topological edge states in parity-time-symmetric quantum walks, *Nat. Phys.* **13**, 1117 (2017).
- [19] S. V. Suchkov, A. A. Sukhorukov, J. Huang, S. V. Dmitriev, C. Lee, and Y. S. Kivshar, Nonlinear switching and solitons in  $\mathcal{PT}$ -symmetric photonic systems, *Laser Photon.* **10**, 177 (2016).
- [20] C. Hang, G. Huang, and V. V. Konotop,  $\mathcal{PT}$  Symmetry with a System of Three-Level Atoms, *Phys. Rev. Lett.* **110**, 083604 (2013).
- [21] J. Sheng, M. Miri, D. N. Christodoulides, and M. Xiao, PT-symmetric optical potentials in a coherent atomic medium, *Phys. Rev. A* **88**, 041803(R) (2013).
- [22] Z. Zhang, Y. Zhang, J. Sheng, L. Yang, M. Miri, D. N. Christodoulides, B. He, Y. Zhang, and M. Xiao, Observation of Parity-Time Symmetry in Optically Induced Atomic Lattices, *Phys. Rev. Lett.* **117**, 123601 (2016).
- [23] P. Peng, W. Cao, C. Shen, W. Qu, J. Wen, L. Jiang, and Y. Xiao, Anti-parity-time symmetry with flying atoms, *Nat. Phys.* **12**, 1139 (2006).
- [24] C. Hang and G. Huang, Parity-time symmetry with coherent atomic gases, *Adv. Phys.: X* **2**, 737 (2017).
- [25] Z. Zhang, D. Ma, J. Sheng, Y. Zhang, Y. Zhang, and M. Xiao, Non-Hermitian optics in atomic systems, *J. Phys. B: At., Mol., Opt. Phys.* **51**, 072001 (2018).
- [26] C. Hang and G. Huang, Weak-light solitons and their active control in a parity-time-symmetric atomic system, *Phys. Rev. A* **91**, 043833 (2015).
- [27] T. F. Gallagher, *Rydberg Atoms* (Cambridge University Press, Cambridge, England, 2008).
- [28] J. D. Pritchard, K. J. Weatherill, and C. S. Adams, Nonlinear optics using cold Rydberg atoms, *Annu. Rev. Cold At. Mol.* **1**, 301 (2013).
- [29] O. Firstenberg, C. S. Adams, and S. Hofferberth, Nonlinear quantum optics mediated by Rydberg interactions, *J. Phys. B: At., Mol., Opt. Phys.* **49**, 152003 (2016).

- [30] C. Murray and T. Pohl, Quantum and nonlinear optics in strongly interacting atomic ensembles, in *Advances in Atomic, Molecular, and Optical Physics* (Academic Press, New York, 2016), Vol. 65, Chap. 7, pp. 321–372.
- [31] C. Yin, Y. He, H. Li, and J. Xie, Solitons in parity-time symmetric potentials with spatially modulated nonlocal nonlinearity, *Opt. Express* **20**, 19355 (2012).
- [32] C. P. Jisha, A. Alberucci, V. A. Brazhnyi, and G. Assanto, Nonlocal gap solitons in  $\mathcal{PT}$ -symmetric periodic potentials with defocusing nonlinearity, *Phys. Rev. A* **89**, 013812 (2014).
- [33] C. P. Jisha, A. Alberucci, and G. Assanto, PT-symmetric nonlocal gap solitons in optical lattices, *J. Nonlinear Opt. Phys. Mater.* **23**, 1450041 (2014).
- [34] D. A. Zezyulin and V. V. Konotop, Small-amplitude nonlinear modes under the combined effect of the parabolic potential, nonlocality and  $\mathcal{PT}$  symmetry, *Symmetry* **8**, 72 (2016).
- [35] L. Li, X. Zhu, H. Li, and T. Lai, Vector solitons in parity-time symmetric lattices with nonlocal nonlinearity, *J. Opt.* **18**, 095501 (2016).
- [36] S.-L. Xu, Y. Zhao, N. Z. Petrović, and M. R. Belić, Spatiotemporal soliton supported by parity-time symmetric potential with competing nonlinearities, *Europhys. Lett.* **115**, 14006 (2016).
- [37] Z. Wen and Z. Yan, Solitons and their stability in the nonlocal nonlinear Schrödinger equation with PT-symmetric potentials, *Chaos* **27**, 053105 (2017).
- [38] Ziauddin, Y. Chuang, and R. Lee,  $\mathcal{PT}$ -symmetry in Rydberg atoms, *Europhys. Lett.* **115**, 14005 (2016).
- [39] W. Demtröder, *Laser Spectroscopy: Basic Concepts and Instrumentation*, 3rd ed. (Springer, Berlin, 2003), Chap. 10.
- [40] Note that we assume all the atoms are initially populated in the state  $|1\rangle$ , and hence the average of the operator  $\hat{O}$  means  $\langle \hat{O} \rangle = \langle G | \hat{O} | G \rangle$ , with  $|G\rangle = |1, 1, 1, \dots, 1\rangle$ .
- [41] Z. Bai and G. Huang, Enhanced third-order and fifth-order Kerr nonlinearities in a cold atomic system via atom-atom interaction, *Opt. Express* **24**, 4442 (2016).
- [42] Expressions of  $\alpha_{jl}^{(1)}$  and  $\alpha_{jl}^{(2)}$  are determined by the corresponding equations given in Appendix A, which are lengthy and hence not listed explicitly in the main text.
- [43] S. Sevinçli, N. Henkel, C. Ates, and T. Pohl, Nonlocal Nonlinear Optics in Cold Rydberg Gases, *Phys. Rev. Lett.* **107**, 153001 (2011).
- [44] V. Arrizón, U. Ruiz, R. Carrada, and L. A. González, Pixelated phase computer holograms for the accurate encoding of scalar complex fields, *J. Opt. Soc. Am. A* **24**, 3500 (2007).
- [45] V. Arrizón, D. Sánchez-de-la-Llave, G. Méndez, and U. Ruiz, Efficient generation of periodic and quasi-periodic nondiffractive optical fields with phase holograms, *Opt. Express* **19**, 10553 (2011).
- [46] Y. Bromberg and H. Cao, Generating Non-Rayleigh Speckles with Tailored Intensity Statistics, *Phys. Rev. Lett.* **112**, 213904 (2014).
- [47] The radius of the blockade sphere,  $R_b$ , is estimated by  $R_b = (|C_6/\delta_{\text{EIT}}|)^{1/6}$ , with  $\delta_{\text{EIT}}$  the linewidth of EIT transmission spectrum (i.e., the width of EIT transparency window), calculated by  $\delta_{\text{EIT}} = |\Omega_c|^2/\gamma_{31}$  for  $\Delta_3 = 0$  and  $\delta_{\text{EIT}} \approx |\Omega_c|^2/\Delta_3$  for  $\Delta_3 \gg \gamma_{31}$ .
- [48] Y. Lumer, Y. Plotnik, M. C. Rechtsman, and M. Segev, Nonlinearly Induced PT Transition in Photonic Systems, *Phys. Rev. Lett.* **111**, 263901 (2013).
- [49] A. W. Snyder and D. J. Mitchell, Accessible solitons, *Science* **276**, 1538 (1997).
- [50] J. Yang, *Nonlinear Waves in Integrable and Nonintegrable Systems* (SIAM, Philadelphia, 2010).